J Mater Sci: Mater Med (2010) 21:109–122
DOI 10.1007/s10856-009-3853-7

Hardness properties and microscopic investigation of crack–crystal interaction in SiO_2–MgO–Al_2O_3–K_2O–B_2O_3–F glass ceramic system

Shibayan Roy · Bikramjit Basu

Received: 15 December 2008 / Accepted: 13 August 2009 / Published online: 3 September 2009

Abstract In view of the potential engineering applications requiring machinability and wear resistance, the present work focuses to evaluate hardness property and to understand the damage behavior of some selected glass–ceramics having different crystal morphologies with SiO_2–MgO–Al_2O_3–K_2O–B_2O_3–F composition, using static micro-indentation tests as well as dynamic scratch tests, respectively. Vickers hardness of up to 5.5 GPa has been measured in glass–ceramics containing plate like mica crystals. Scratch tests at a high load of 50 N in artificial saliva were carried out in order to simulate the crack–microstructure interaction during real-time abrasion wear and machining operation. The experimental observations indicate that the novel "spherulitic-dendritic" shaped crystals, similar to the plate like crystals, have the potential to hinder the scratching induced crack propagation. In particular, such potential of the 'spherulitic-dendritic' crystals become more effective due to the larger interfacial area with the glass matrix as well as the dendritic structure of each mica plate, which helps in crack deflection and crack blunting, to a larger extent. While modest damage tolerant behavior is observed in case of 'spherulitic-dendritic' crystal containing material, severe brittle fracture of plate like crystals were noted, when both were scratched at 50 N load.

1 Introduction

In last few decades, SiO_2–MgO–Al_2O_3–K_2O–B_2O_3–F glass ceramic system received wider attention due to their high machinability, which results in an increased versatility of the finished shape and thereby, widening numerous possibilities for industrial application [1, 2]. Mica based machinable glass–ceramics in the K_2O/Na_2O–B_2O_3–Al_2O_3–SiO_2–MgO–F system contains randomly oriented interlocked and sheet-like fluorphlogopite mica crystals in the alumino-borosilicate glass matrix [3]. From the microstructural engineering point of view, a large number of studies have reported the crystallization behavior of various glass–ceramic materials. In the crystallization process of mica based glass–ceramics, the first crystal phase to form at relatively low temperature is called chondrodite. Chondrodite successively forms norbergite crystals at higher temperature from which the final crystal phase i.e. fluorophlogopite forms epitaxially [4]. The influence of different fluorine source on the crystallization behavior of R_2O–MgO–Al_2O_3–B_2O_3–SiO_2–F is reported by Cheng et al. [5]. While the addition of NaF is reported to result in precipitation of large dendrite shaped norbergite crystal, plate like fluorophlogopite is formed with MgF_2 addition. Various studies have reported different crystal morphologies in this glass–ceramics. Hoche et al. reported the growth of highly defective mica plates along with norbergite in an extruded glass–ceramic [6]. In another interesting study, Gebhardt et al. reported the formation of cabbage shaped mica crystal aggregates in micaceous glass system K_2O–Na_2O–Al_2O_3–SiO_2–MgO–F [7]. Although different crystal morphologies, as mentioned above, are reported in literature, their mechanical properties/scratch resistance property is not widely investigated.

As far as the micromechanics of mechanical response is concerned, the unique pseudo-ductility property and consequent machinability arises due to the crystal structure of fluorophlogopite, which contains a cleavage plane and preferred direction of fracture [8]. It needs to be mentioned

S. Roy · B. Basu (✉)
Department of Materials and Metallurgical Engineering, Indian Institute of Technology, IIT-Kanpur, Kanpur, India
e-mail: bikram@iitk.ac.in

here that the concept of pseudo-ductility essentially means the ductile-like behavior due to characteristic crystal structure, as opposed to dislocation induced ductile deformation in metallic materials. If some crystal planes, because of favorable ionic arrangements, can be sheared easily, then such material can behave more like 'pseudo-ductile' manner. Structurally, fluorophlogopite is a trioctahedral fluoromica, composed of 2:1 negatively charged layers, that are connected via large, positively charged interlayered alkali (Na/K) ions [3, 9]. The [001] crystallographic plane of the mica crystal is reported to be the preferred direction of fracture, because the alkali ions, sandwiched between the three-layer packets, do not establish a compact connection [1]. The characteristic microstructure of machinable glass–ceramics facilitates micro-fracture along the weaker mica–glass interfaces and mica basal planes. This occurs preferably when the crack propagation direction is closely aligned with the direction of tangential stress [10, 11].

Lawn et al. [12] reported that the deformation of glass–ceramics occurs in the form of an expanding microcrack damage zone at the Hertzian contacts, instead of the usual single propagating microcrack (brittle ceramics). Baik et al. [13] observed that the microhardness decreases and machinability increases with crystals having higher aspect ratio and crystallinity. This is because of the fact that high connectivity amongst the mica crystals leads to enhanced plastic deformation. When the mica crystals are finer (4.5 μm or less), the strength of the glass–ceramics increases with the mica plate diameter, because of the thermal stresses, arising from the thermal expansion mismatch between the larger mica plates and the residual glass [14]. It has been observed by Grossman et al. [14] that glass–ceramics containing as little as 30 vol.% of mica may be machinable, if the aspect ratio of the crystals is high enough to cause a high degree of interlocking. Amongst various mechanical testing techniques, scratch testing is often used to understand the abrasion resistance and machining operations, more realistically, than static tests (e.g. indentation hardness). Xu et al. [15] observed that the scratching produces radial-median cracks in the base glass. In a different work, Flanders et al. [16] demonstrated that scratch tool/environment interactions were significantly more important than material composition/environment interactions, which imply that environmentally enhanced machining processes are relatively material independent.

Recently, we have demonstrated how one can obtain unusual combination of spherulitic and dendritic growth morphology of mica crystals with high volume fraction by optimizing the heat treatment conditions in the SiO_2–MgO–Al_2O_3–K_2O–B_2O_3–F glass–ceramic system [17–19]. This combination of both crystallization habits leads to a characteristically different crystal shape than the typical "house of cards" mica plates, when SiO_2–MgO–Al_2O_3–K_2O–B_2O_3–F base glass is isothermally heat treated at 1,000°C for more than 4 h. Heat treatment times of 8, 12, 16, 20 and 24 h were used in our previous study to produce this typical 'spherulitic-dendritic' structure [17–19]. In the present study, the effect of crystal volume fraction and different morphologies of the characteristic crystalline phases on mechanical property of some selected glass–ceramic samples is critically evaluated by micro-indentation and scratch testing. Scratch tests in artificial saliva at high load (50 N) are carried out on the heat treated glass–ceramic samples in order to simulate the abrasion wear and machining operation. Much focus has been provided to understand the mechanisms of crack/crystal interaction using electron microscopy technique.

2 Materials and methods

2.1 Material preparation

In the present investigation, the SiO_2–MgO–Al_2O_3–K_2O–B_2O_3–F glass–ceramic system was used and the composition of the base glass was closely similar to the commercial composition available in that system (MACOR®, Corning Glass Ltd.). The silica gel, used in this work was ultra pure and contained more than 1% humidity. The composition of the starting precursor materials is provided in Table 1. This composition is obtained from the previous work of Guedes et al. [20] and is rechecked from www.precisionceramics.co.uk. Initially, the base glass was prepared at 1,500°C in two steps i.e. first, the frit was prepared by quenching the melt in water and then by subsequently remelting the frit and quenching in air. This procedure is followed and also reported in earlier works for better homogenization of the constituent elements [6, 7, 21]. For frit preparation, the melt was kept at 1,500°C for 1 h and for base glass plate preparation; the soaking time was 6 h. For both the cases, the heating rate was 5°C/min and the base glass plate was

Table 1 Composition of base glass (AR corresponds to analytical reagent grade)

Starting materials	Oxide constituent	Wt%	Comments
Silica gel in powder form	SiO_2	46	60–120 mesh, AR grade
White tabular alumina	Al_2O_3	16	99.9% pure, $d_{50} \leq 1$ μm, AR grade
MgO powder	MgO	17	99% pure, AR grade
K_2CO_3	K_2O	10	99.9% pure, AR grade
Boric acid (H_3BO_3)	B_2O_3	7	99.5% pure, AR grade
NH_4F	NA	4	95% pure, AR grade

Table 2 Elemental composition of base glass and crystal phase for differently processed materials (wt%)

	Temperature variation batches containing plate shaped crystals (1,120°C, 4 h)		Temperature variation batches containing "spherulitic-dendritic "shaped crystals (1,000°C, 12 h)	
	Base glass composition (wt%)	Crystal composition (wt%)	Base glass composition (wt%)	Crystal composition (wt%)
O	25.19	25.29	40.42	28.06
F	0.38	0.95	10.69	1.66
Mg	4.28	4.2	5.47	17.29
Al	13.13	11.54	8.57	11.72
Si	48.31	49.76	27.9	38.34
K	8.72	8.26	6.95	2.92

cooled to room temperature from 1,500°C in 15–20 min. The base glass was optically transparent after melting and no visible defects in the base glass were observed. TGA study (not shown) showed a weight loss of around 20–25% on heating and subsequently SiO_2 and NH_4F were added 25% in excess to what was theoretically required, to the precursor mix in order to compensate for the volatile material loss.

The base glass plate was cut into small pieces of 2.5 cm × 2 cm × 1 cm using a diamond blade cutter (Isomet Low Speed Saw, Buehler, Germany). Three specimens were used for mechanical property measurements from each heat treatment schedule. The crystallization heat treatments were done both by varying temperature from 1,000°C to 1,120°C with 40°C temperature interval for a constant soaking time duration (i.e. the holding time at the concerned heat treatment temperature) of 4 h and by varying the soaking time duration from 4 h to 24 h with 4 h time interval at constant temperature of 1,000°C. During the heat treatment experiments, the heating rate and cooling rate remained constant at 10°C/min and 3.5°C/min, respectively. The chemical compositions in terms of the elements present (wt%) for differently processed materials are shown in Table 2. This elemental composition is obtained by SEM–EDS (Energy Dispersive Spectroscopy) method. Since this method is not very effective for light elements, boron is omitted from the list as it introduces large amount of error. It is important to note that during crystallization of the base glass, elemental separation occurs between the base glass and the crystal. Therefore, the composition is presented separately for the base glass and the crystal.

2.2 Microstructural characterization

After heat treatment, the glass–ceramics samples were smoothly polished using diamond paste (from 9 μm to 0.25 μm). The polished surfaces are etched with 12% HF for 5 min to reveal the microstructure. Furthermore, the microstructural characterization of these etched and polished samples was carried out using electron microscope-energy dispersive spectroscopy (SEM–EDS)[1] and both secondary as well as backscattered electron images were taken. The scanning electron microscopy images were analyzed using Image-Pro-Plus software for crystal volume fraction calculation. The software was calibrated using a control material with known crystal volume fraction (measured via density determination [22]) prior to the image analysis of the heat treated specimens. At least 25 micrographs of each set of specimens were used for image analysis and volume fractions were calculated with 95% confidence level (see Table 3). The study of phase assemblage in the heat treated specimens was performed using the XRD[2] technique on the polished surfaces at scan rate of 0.05°/min with a fixed counting time of 3 s. All the microstructural characterizations and phase evaluation studies (XRD) were performed on the bulk of the samples after removing at least 3–5 μm of the surface layer in order to investigate the effect of different heat treatment conditions on the bulk microstructure development. Various JCPDS file numbers: 340158, 150776 and 330853 were used to identify the characteristic XRD peaks for Potassium fluorophlogopite, Mullite ($Al_6Si_2O_{13}$) and $MgAl_2O_4$ spinel phases, respectively.

Table 3 Vickers Micro hardness and crystal volume fraction of heat treated glass–ceramics samples

Heat treatment conditions	Vickers microhardness (GPa)	Crystal volume fraction (%)
1,040°C, 4 h	5.5 ± 0.5	59.2 ± 2.0
1,080°C, 4 h	5.2 ± 0.3	46.1 ± 3.3
1,120°C, 4 h	4.8 ± 0.6	46.8 ± 2.9

[1] FEI QUANTA 200, The Netherlands.

[2] Isodebyeflex 2002, USA.

2.3 Mechanical property characterization

Two sets of experiments, one of evaluating the mechanical property (Hardness) with Vickers indenter and the other set involving scratch tests (crack–crystal interaction) of the heat-treated samples have been performed in the present study. Before taking the indentations, the samples were smoothly polished using diamond paste (from 9 μm to 0.25 μm) and etched with 12% HF for 5 min. Etching was found useful in terms of revealing the microstructure, which further helped in understanding the indentation induced damage resistance behavior of the glass–ceramic material (both the crystals and the glass matrix). Micro-indentations were taken using microhardness tester,[3] equipped with a conical Vickers's indenter. An indent load of 160 g was applied during indentation tests. At least 20 indentations were taken for each of the heat-treated samples and final hardness value was reported as the average of all the measurements with 95% confidence level (see Table 3). The indentations were observed under SEM and the two diagonals of each indentation were measured and averaged. Hardness values were calculated using the following relation [23],

$$H_v = 1.854 \times P/D^2$$

where H_v is the Vickers hardness number (HV) in kg/mm^2, P is the normal load in kg, and D is the length of the diagonal of the indentation in mm. To convert the H_V into GPa, the following relation was used,

$$H_v(\text{GPa}) = 9.81/1000 \times H_v$$

The idea of carrying the scratch test was to study the resistance offered by the crystals towards the scratch induced radial/median cracks. Such a study would be helpful to predict the machining as well as the abrasion resistance behavior of glass–ceramic samples. In the present investigation, scratch tests of the heat treated glass–ceramic samples were carried out using a specially designed scratch tester,[4] equipped with a conical Rockwell diamond indenter. The equipment was attached to a CCD camera and a sample pad. By a stepper motor, the indenter was made to move unidirectionally over the flat polished sample with a fixed scratching speed of 0.5 mm/s and a constant normal load of 50 N was applied for a stroke length of 5 mm. Such combination of testing parameters was chosen in order to understand and compare the scratch induced damage response of glass–ceramics, containing different characteristic shaped crystalline phase under the extreme loading conditions. The scratch tests were performed using freshly prepared artificial saliva solution. In recent times, these glass–ceramic materials appear to be the candidate materials for fabricating dental restorations, as the main problem of all the dental ceramics is the premature failure during in vivo operational conditions due to the presence of surface flaws or cracks, resulting during complex CAD/CAM operation [10]. The prime motivation of the selection of such testing solution was therefore to simulate the actual working condition i.e. the oral environment for this material when used in dental restorative purpose. Artificial saliva (AS) was prepared using the composition obtained from the work of earlier researcher [16, 24]. The composition of AS includes NaCl (0.4 g), KCl (0.4 g), $CaCl_2$–2H2O (0.795 g), $NaH2PO_4 \cdot 2H_2O$ (0.78 g), $Na_2S \cdot 9H_2O$ (0.005 g), Urea (1.0 g). All the chemical reagents, in appropriate amount, were mixed in 1,000 ml of distilled water using a magnetic stirrer at a temperature of 60°C and a speed of 40 rpm for 30 min. Subsequently, it was cooled and kept in straight, airtight glass bottle at 40°C for not more than 1 month. pH measurement was done using a dual channel 'pH/Ion/Conductivity Meter'.[5] Relative viscosity (n/ndw, ndw being viscosity of distilled water) of artificial saliva solution was measured using the well-known 'Ostwald Viscometer'. The pH of artificial saliva was 6.2; while the relative viscosity was measured to be 1.05. The microstructure of the scratched surface was investigated using scanning electron microscopy technique after etching with 12% HF solution for 5 min.

3 Results

3.1 Microstructure of glass–ceramics

XRD analysis of the heat-treated samples was carried out in order to identify the crystal phases (see Fig. 1). All the temperature variation (representative sample, heat treated at 1,040°C and 1,120°C for 4 h) and the time variation batches (representative samples, heat treated at 1,000°C for 4 h and 24 h) show the dominant presence of flurophlogopite as the main crystalline phase. The sample, heat treated at 1,000°C for 4 h, did not show any detectable bulk crystal formation, as can be seen from the broad diffuse peak, indicative of the lack of crystallinity and predominant presence of glassy phase. This is further confirmed by electron microscopy images taken from the bulk of the sample (discussed later), where no crystalline phase can be seen and only glassy matrix is visible. Also, the XRD analysis of the sample heat treated at 1,120°C for 4 h shows the additional presence of Mullite ($Al_6Si_2O_{13}$) and spinel ($MgAl_2O_4$) phases. Nevertheless, the peak intensity of fluorophlogopite (FPP) remains highest, indicating

[3] Carl Zeiss Jena, Germany.

[4] TR 101, Ducom, Bangalore, India.

[5] PC5500, Eutech Instruments, USA.

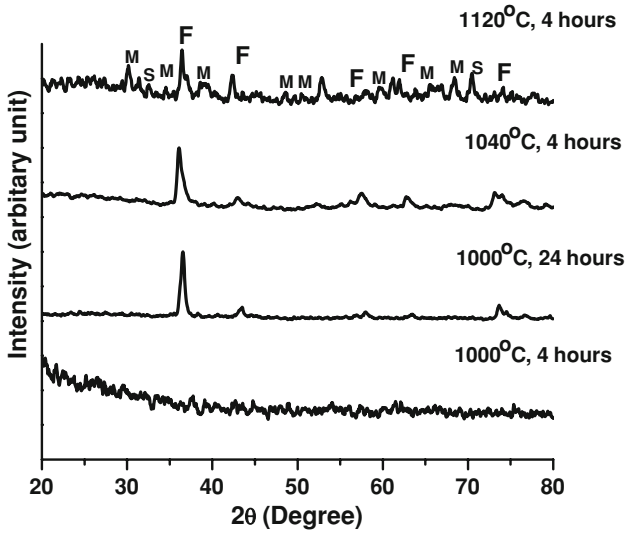

Fig. 1 XRD spectra taken from the polished surface at the bulk of the heat treated samples ('F' stands for Fluorophlogopite, 'M' for Mullite and 'S' for spinel). Sample heat treated at 1,000°C for 4 h represents the base glass characteristics. Similarly, samples heat treated at 1,040°C for 4 h and 1,000°C for 24 h represent the temperature and time variation batches containing the maximum volume fraction of crystalline phase, respectively

predominant presence of FPP phase. The detailed microstructural analysis by electron microscopy technique of different heat-treated samples at varying temperature as well as varying time is presented in Figs. 2 and 3. The samples heat-treated at 1,000°C for 4 h show no sign of detectable bulk crystal formation (see Fig. 2a). However, the samples heat treated at 1,040°C, 1,080°C and 1,120°C for 4 h show the usual microstructure of plate like interlocked mica flakes, randomly oriented in the glassy matrix (see Fig. 2b–d). The characteristic features include a width of 1–1.5 μm, average length of 10–15 μm and interlocking crystal arrangement. The interlocking nature is more visible in Fig. 2e, which shows the connectivity of the mica plates. SEM–EDS analysis reveals the strong presence of Si with moderate and comparable intensity peaks of Mg and Al in the crystalline phase (see Fig. 2f). Also, for the sample heat treated at 1,120°C for 4 h, a needle shape is observed at the end of mica plates (see Fig. 2e).

On the other hand, the morphology of the crystal phase in time variation samples is quite interesting. The microstructural evolution of samples heat-treated at 1,000°C for varying time period is presented in Fig. 3. The important observation is that a typical crystalline morphology with a number of mica plates radiating from a central nucleus constitutes as the major microstructural phase (see Fig. 3c, f). Such morphology of the crystal phases is common for all the time variation batches i.e. samples heat treated at 1,000°C for 8, 12, 16, 20 and 24 h. At the end of each of the mica plates, a characteristic 'tree leave' shaped structure is seen (see Fig. 3e). Closer observation of Fig. 3g reveals the stacking of mica plates in the formation of mica rods. In the sample heat-treated for 24 h, the characteristic crystal morphology with radiating mica plates from the central nucleus is clearly visible (see Fig. 3f). SEM–EDS analysis reveals comparably higher presence of Mg and Al in these crystals than that of the crystals formed in temperature variation samples (see Fig. 3a). More details on the microstructural analysis of the studied glass–ceramics can be found elsewhere [17–19].

The crystal volume fraction of all the batches is measured using the image analysis of the micrographs taken by SEM. For the glass–ceramics samples heat treated at 1,000°C for 4 h, the volume fraction of the crystals can not be measured, as it is completely glassy without any detectable sign of crystal formation. For other samples of temperature variation batches, glass–ceramics heat treated at 1,040°C for 4 h shows the maximum crystal phase formation of more than 55% by volume, whereas the other two batches i.e. samples heat treated at 1,080°C and 1,120°C for 4 h, exhibit lesser amount of crystal formation of around 45–48% (see Fig. 4). The crystal volume fraction in the two batches heat treated at 1,080°C and 1,120°C for 4 h are almost comparable. For time variation samples, however, crystal volume fraction varies almost linearly in a wide range from nearly 20% for 8 h soaking time sample to nearly 70% for 24 h soaking time sample (see Fig. 5). Such a linear increase in crystallization with time, as observed with spherulitic-dendritic morphology, is consistent, with the crystal fibrils always moving into the surrounding glass of constant composition or in other words, growing under steady state conditions with a constant radius of curvature at the growth front [25].

3.2 Hardness properties

For the glass–ceramics sample, heat treated at 1,000°C for 4 h, hardness could not be measured. This is because of the fact that the indented zones are heavily deformed (not shown) and diagonal lengths were not measurable at an indent load of 160 g. Figure 4 plots the hardness values along with the crystal volume fraction for the three temperature variation batches (all soaked for 4 h) e.g. samples heat treated at 1,040°C, 1,080°C and 1,120°C. The error bars in the hardness data represent the standard deviation of all the measured values around the average for a set of 20 (at least) indentations. Since the error bars are overlapping, it is appropriate to comment that the hardness values after heat treatment at 1,040°C, 1,080°C and 1,120°C vary within statistical deviation and the average hardness is around 5 GPa.

Figure 6a shows the electron microscopy image of a representative Vickers indentation impression acquired on

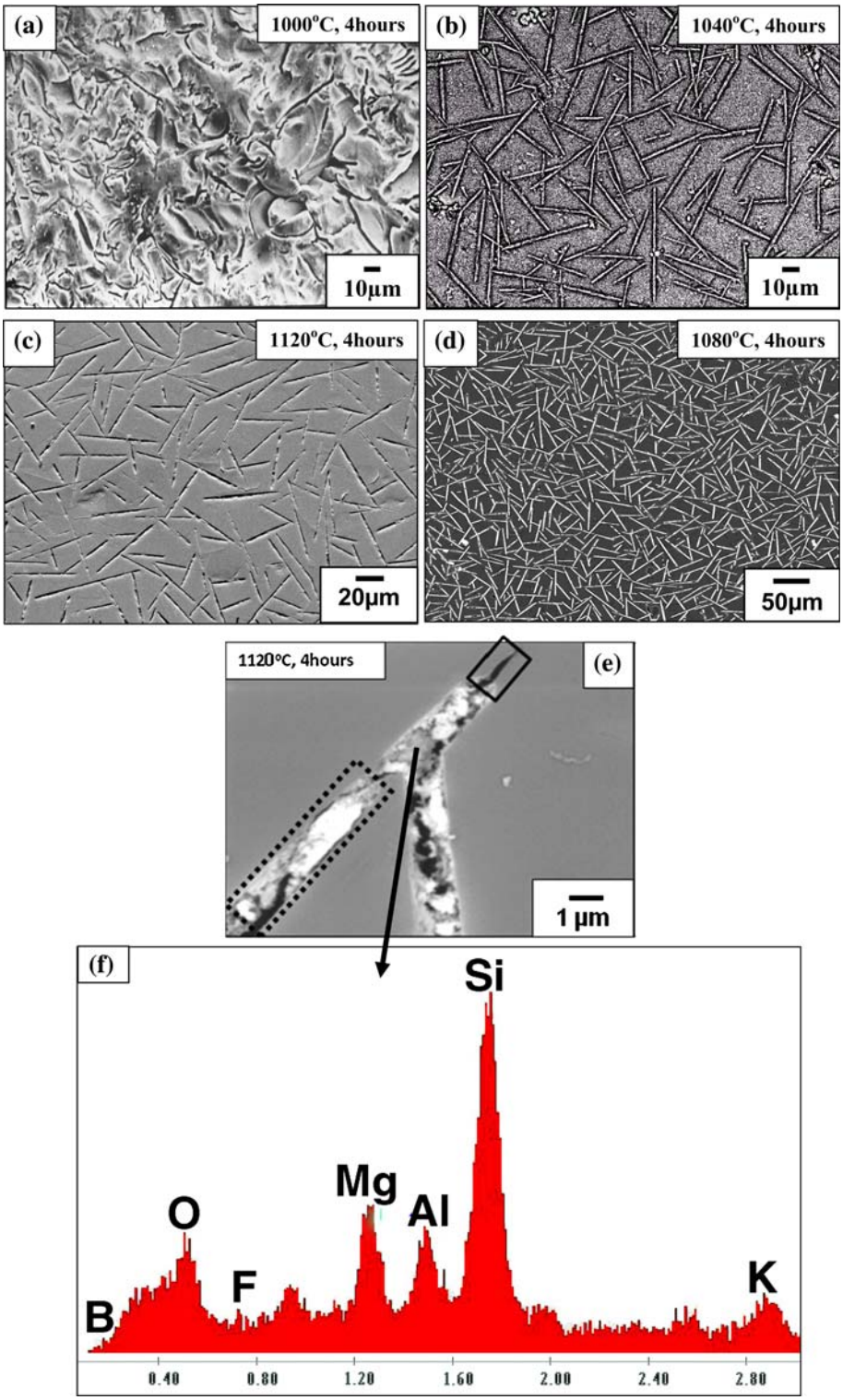

Fig. 2 SEM micrographs of samples heat treated at **a** 1,000°C, 4 h, showing no sign of crystallinity, **b** 1,040°C, 4 h, **c** 1,120°C, 4 h, and **d** 1,080°C, 4 h showing usual randomly oriented interlocked mica flake, **e** 1,120°C, 4 h showing the interlocking between individual mica flakes and a characteristic needle shape (possible sign of mullite formation) at the end of the mica plate; the mica crystal appears as rectangular plate in two dimension, which is being shown with dotted line in the micrograph and the mullite crystal that forms in needle shape at the end of the mica crystals is shown in solid lines, and **f** corresponding EDS spectrum of the characteristic crystal phase. The first micrograph is a secondary electron image and the rests are all backscattered electron images

the sample heat treated at 1,120°C for 4 h. All such impressions were distinct and easily measurable. The observations on multiple indentations reveal that the radial-median cracks are not propagated from all the indent corners. This makes the measurement of toughness by indentation method impossible and alternative toughness measurement technique will be adopted in our future investigation. The observation of stable indents (no

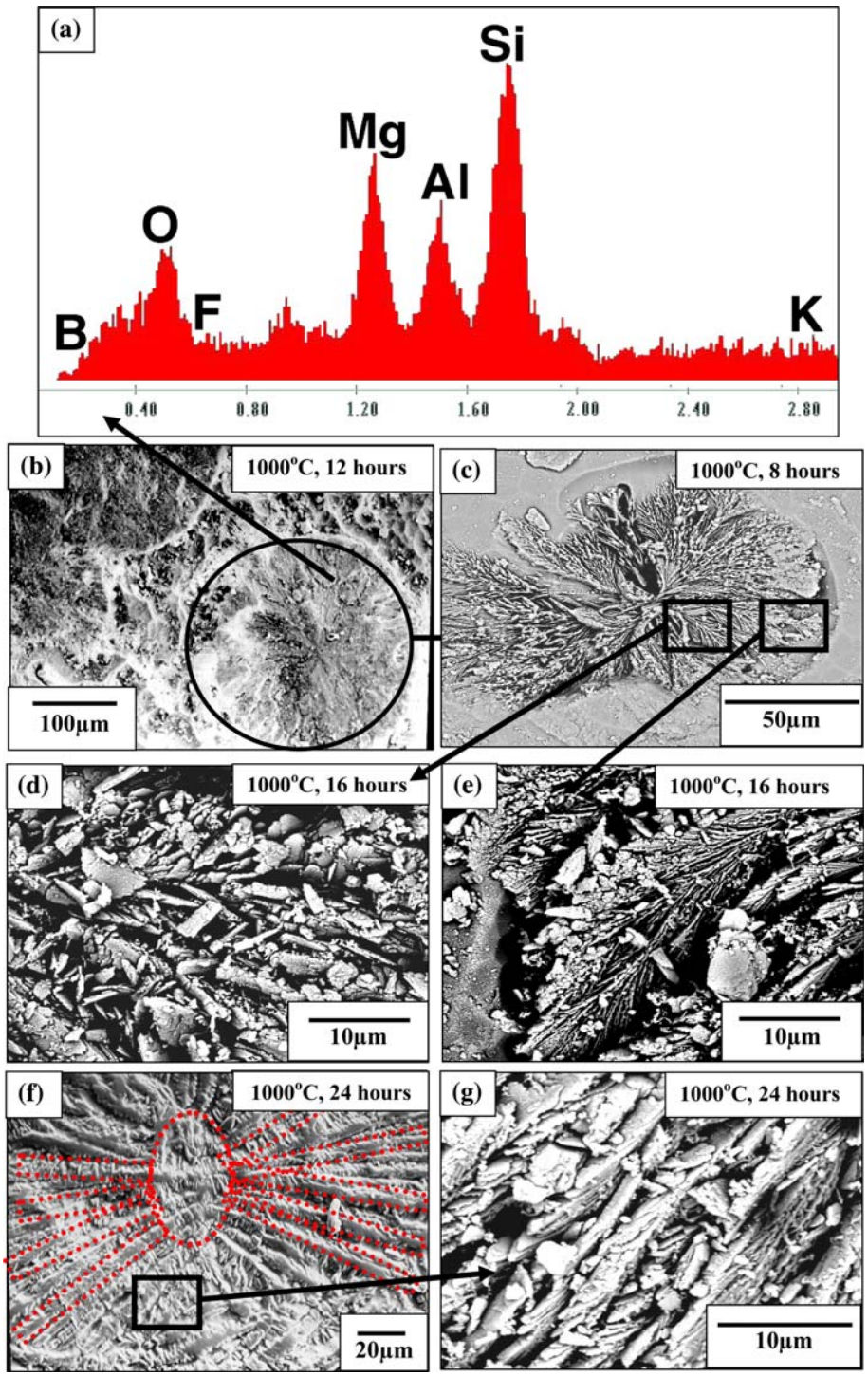

Fig. 3 SEM micrographs of time variation samples heat treated at 1,000°C showing **a** EDS diagram of the crystal phase (Soaking time 12 h), **b** corresponding SEM image showing crystals evolved from spherical droplets (Soaking time 12 h), **c** single "Spherulitic-dendritic "shaped crystals (Soaking time 8 h) **d** Scattering of mica plates over the crystal phase (Soaking time 16 h), **e** "Tree leave" structure at the end of each mica plate (Soaking time 16 h), **f** Individual 'spherulitic-dendritic' crystal showing different length of different mica rods; the 'spherulitic-dendritic' like shape (central nucleus and individual mica plates elongated from this nucleus) is shown with dotted lines (Soaking time 24 h) and **g** Stacking of mica plates forming mica rods (Soaking time 24 h). The first micrograph is a secondary electron image and the rests are all backscattered electron images

chipping or no spalling around indent edges) and the presence of the radial cracks appear to support the theory of 'quasi-ductility' in this glass–ceramics [26].

In case of the time variation batches, our observations indicate that the Vickers indentation size (diagonal length ~10 µm) is markedly smaller than the size of the 'spherulitic-dendritic' crystals as well as the inter-crystal spacing in the time variation samples, Therefore, it is possible that the indents either fall over the crystals directly or onto the glass matrix. In either case, the indentation was heavily damaged and diagonal length was hard to measure. In order to provide an evidence of such observations, one such example of a distorted indentation is provided in Fig. 6b (inset). On some occasions, e.g. for the sample, heat-treated at 1,000°C for 8 h, the indent diagonals could be measured with certain difficulties on electron microscopy images and

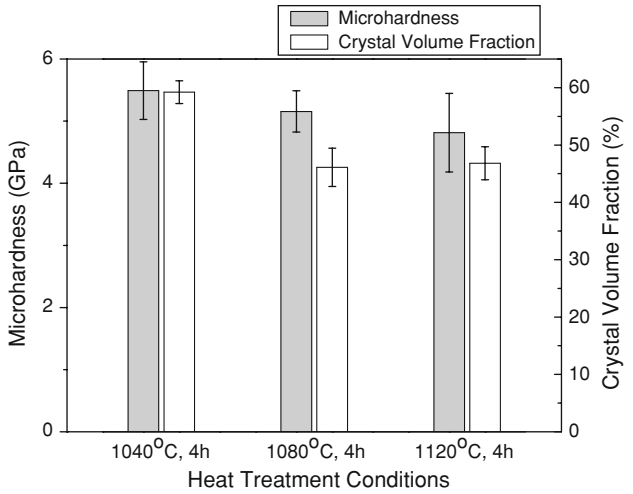

Fig. 4 Correlation of micro-hardness with the volume fraction of crystalline phase for the investigated glass–ceramics

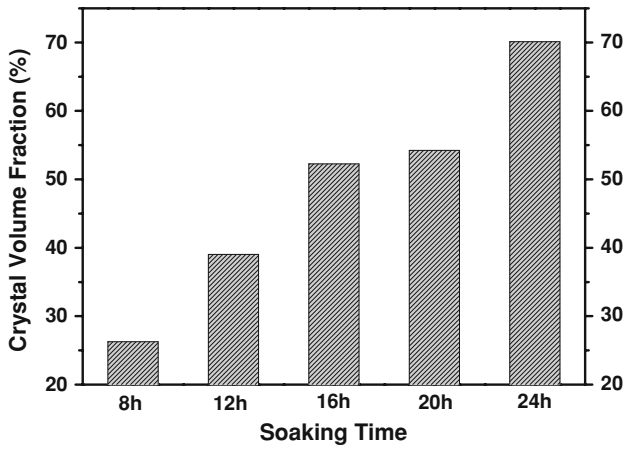

Fig. 5 Plot of crystal volume fraction in glass–ceramic heat treated for various soaking time (8–24 h) at 1,000°C

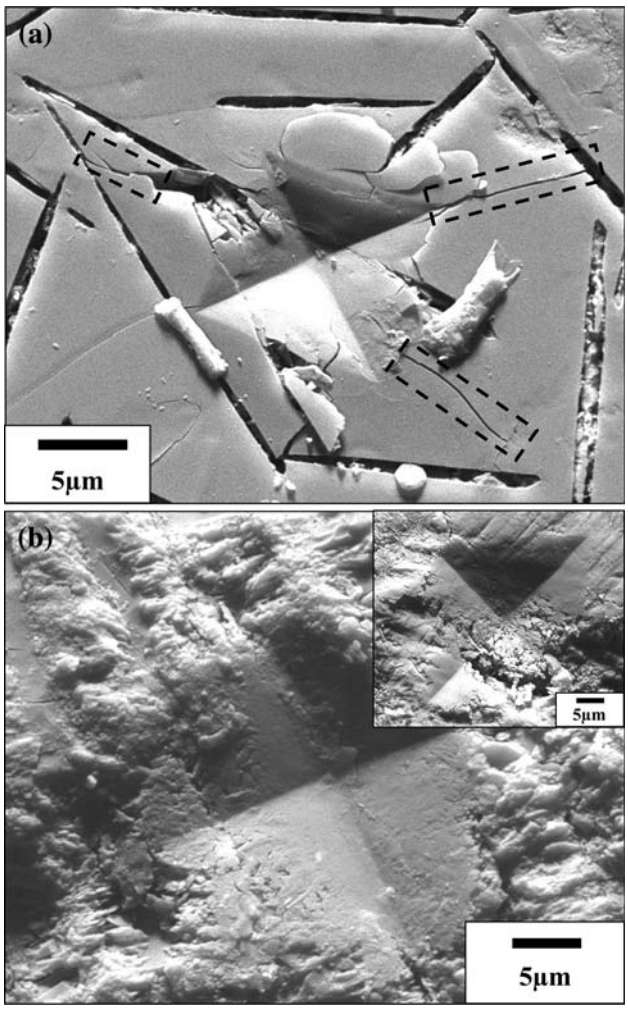

Fig. 6 **a** SEM image (BSE image) of a Vickers indent on glass–ceramic, heat treated at 1,120°C for 4 h showing almost perfect indentations and radial cracks emanating from the edge of the indentation (the dashed boxes are showing the radial cracks evolved during indentation). **b** Representative image of indented sample (SE image), heat treated at 1,000°C for 8 h. Inset: Indentation image of sample, heat treated at 1,000°C for 20 h. The indent load was 160 g

the measured hardness is around 5 GPa (see Fig. 6b). It should however be reiterated that consistent hardness measurements for all the time-variation batches were not possible in a reproducible manner. The evidence of increased microfracture and material dislodgement around Vickers indentation impression has been commonly noted, irrespective of crystalline volume fraction in glass–ceramic samples containing spherulitic-dendritic crystals. Similar observations were also recorded for tetrasilisic fluoromica glass–ceramics, containing 50% crystalline phase [27].

It is important to mention here that a number of attempts to measure indentation fracture toughness using vickers indentation method was failed to provide reproducible and consistent values for the "spherulitic-dendritic" crystal containing microstructure. At very low indent loads, the cracks are not distinctly visible to emanate from all the indent corners. On the other hand, at larger indent load, the extensive indent induced damage is observed, making any estimate of fracture toughness unacceptable. Also, any attempt to prepare SEVNB test sample to measure long crack toughness measurement was not fruitful, largely because of the fact that such sample preparation method does not able to produce sample with acceptable notch geometry as a result of several micro-fractures.

3.3 Crack–microstructure interaction during scratch test

Detailed microstructural observations of the scratched surfaces (top view) were carried out using electron microscopy in order to understand the dominant mechanisms of material

removal as well as scratch–microstructure interaction in glass–ceramics, having two distinctly different crystal morphologies. Since the crack–microstructure interaction is earlier investigated in SiO_2–MgO–Al_2O_3–K_2O–B_2O_3–F glass–ceramic system containing classical 'house of cards' microstructure [10, 11, 28]; much effort, in the present work, is put forward to understand such interaction in glass–ceramics, containing 'spherulitic-dendritic' shaped crystals. Figure 7 shows the interaction of scratch induced crack propagation with the microstructural features in the temperature variation samples (containing usual plate like mica crystals) after scratching in saliva. Interesting observations include the interaction of scratch induced cracks with the crystals leading to crack deflection and subsequent spalling/pull-out of the glass matrix. It has been additionally observed that if a crystal is present on the path of crack propagation, the cracks will try to propagate along the crystal–glass interface, which is weaker than the crystal. Thus, the de-bonding of crystal/glass interface consequently provides a low energy path for crack propagation (see Fig. 7a). If, however, the crack propagation causes the crystals to fracture, the fracture always occurs along specific cleavage plane along a particular direction (see Fig. 7b).

Figure 8 shows the interaction of the crystals with scratch induced cracks, in time variation samples, consisting of the unique 'spherulitic-dendritic' shaped crystals. Like the plate like mica crystals in the temperature variation samples, the 'spherulitic-dendritic' crystals also demonstrate their ability to deflect the propagating crack along the crystal–glass interface. However since the 'spherulitic-dendritic' crystals are larger in size than the plate like one, the deflection occurs to a greater extent (see Fig. 8a). An interesting observation is that the cracks actually try to chip off the crystals along the interface from the glassy matrix, rather than fracturing them (see Figs. 8b, 9a). Figure 8b shows the evidence of a 'spherulitic-dendritic' crystal, lying on the path of scratching without any visible bulk-fracture. In the present case, the scratching load is quite high (50 N) and yet importantly, the crystal, being directly on the path of the indenter, is damaged to a limited extent. Also, a plastic-like impression or quasi ductility of spherulitic-dendritic crystal, as evident from the localized relief of the crystal, is observed.

4 Discussion

The hardness property and the crack–microstructure interaction behavior of the investigated glass–ceramics can be explained in the light of the microstructural differences, primarily in terms of crystal morphology.

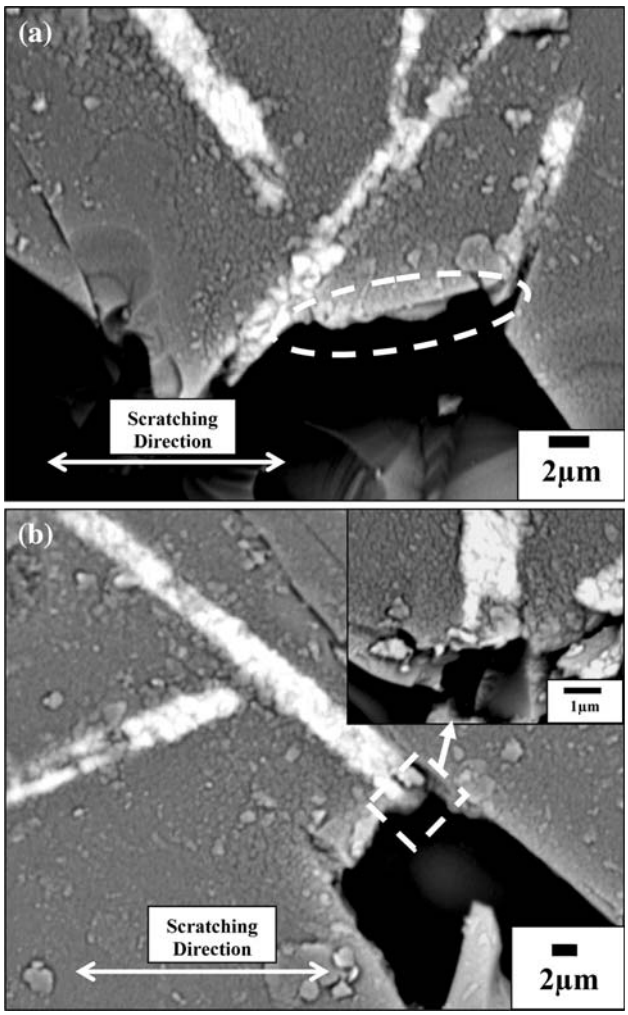

Fig. 7 Interaction of the scratch induced crack with "plate" like crystals (bright contrast phase) in the mica based glass–ceramic sample (heat treated at 1,120°C for 4 h) in artificial saliva environment, when 50 N load was applied on the scratch indenter. While the interaction of scratch induced cracks with the crystals leading to crack deflection along the weak glass/crystal interface and subsequent spalling/pull-out of the glass matrix (*shown with dotted line*) can be seen in (a); the cracking of the crystals along definite cleavage planes (*shown with dotted line*) can be seen in (b) and (b Inset)

4.1 Hardness property

As has been discussed in greater details elsewhere [17–19], the anisotropic growth dominates for temperature variation batches, whereas epitaxial growth along certain crystallographic directions other than the most preferable one as well as the dendritic growth phenomena are likely to be the dominant mechanisms for the crystallization in time variation batches. In Fig. 4, both the hardness and crystal volume fraction are plotted simultaneously. Looking closely the error bars, it is evident that the crystal volume fraction decrease when the heat treatment temperature

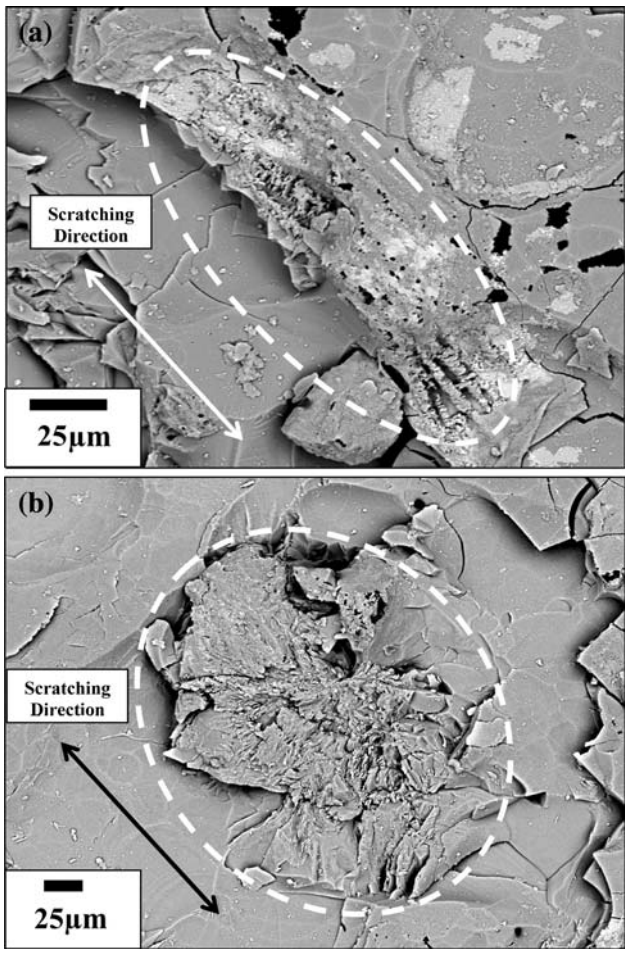

Fig. 8 SEM images revealing interaction of the propagating cracks with "spherulitic-dendritic "shaped crystals in the sample heat treated at 1,000°C for 16 h and scratched in artificial saliva environment at 50 N load, **a** showing evidence of crack deflection and subsequent spalling/pull-out of the glass matrix (*shown with dotted line*) by the crystals around scratched track, and **b** showing relatively undamaged spherulitic-dendritic crystal lying directly on the scratching pathway (*shown with dotted line*)

increases from 1,040°C to 1,080°C and subsequently remains almost constant after heat treatment at 1,120°C. Quantitatively, not statistically correlated though, both the hardness and crystal volume fraction follow closely, The glass–ceramic sample, heat treated at 1,040°C for 4 h contains the highest amount of crystals in the glassy matrix (see Fig. 4) and consequently, its hardness is found to be noticeably higher than other temperature variation batches. Other than the amount of crystal present, the aspect ratio and interlocking between the crystals are reported to play an important role in determining the hardness. Crystals with larger aspect ratio i.e. longer crystals are able to form an effective interlocking [13]. More amount of interlocking in the glass–ceramic material with larger volume fraction of crystals helps in enhancing the deformation of the

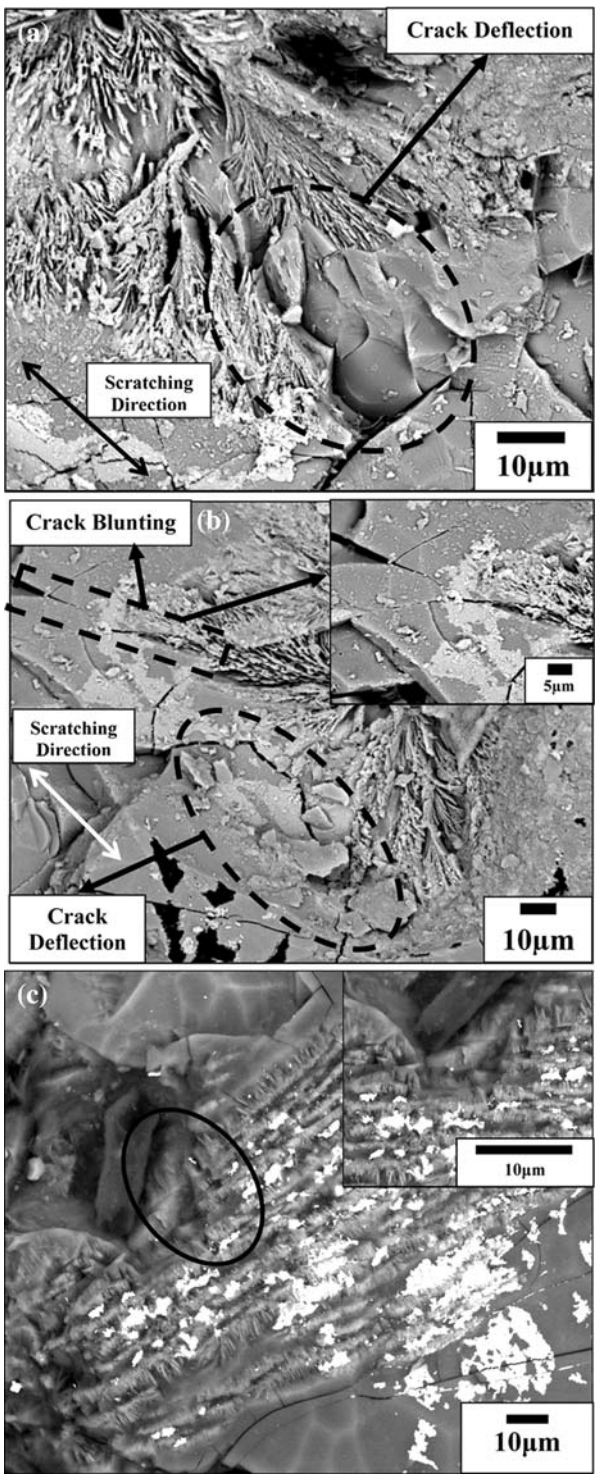

Fig. 9 SEM images revealing the interaction of scratch induced cracks with "spherulitic-dendritic" crystal phase helping in crack blunting and crack deflection (*shown with dotted line*) in the sample heat treated at 1,000°C for 20 h in artificial saliva environment, when 50 N load was applied on the scratch indenter (a, b). **b** inset: crack blunting by the crystal at higher magnification. **c** Interaction of scratch induced cracks with the bundle of mica plates in the middle part of the composite structure of "spherulitic-dendritic" crystals. **c** inset: closer observation of circled region of **c**

Table 4 A comparison of hardness of presently investigated GC with that of earlier developed GCs

Material	Heat treatment conditions	Hardness (GPa)	Reference
Tetrasilisic fluoromica containing Dicor/MGC	>1,000°C	2.7–3.6	Peterson et al. [27]
$8SiO_2$–$3Al_2O_3$–$3MgO$–$3MgF_2$–$(1-z)BaO$–zK_2O–sLi_2O ('z' either 1 or 0 and 's' either 0.5 or 1.0)	1,000–1,250°C	2.1–3.2	Henry et al. [29]
Mica–apatite glass–ceramics, containing 20% and 30% fluoroapatite [$Ca_{10}(PO_4)_6F_2$] crystalline phase	–	2.8 (20% apatite) and 4.8 (40% apatite)	Taruta et al. [30]
Commercial Macor material	–	~3	Davis et al. [31]
SiO_2–MgO–MgF_2 (MAS) glass–ceramics	1,050°C	4–7	Goswami et al. [32]
MgO–Al_2O_3–SiO_2–TiO_2	1,080°C, 3 h	9.5	Wange et al. [21]
Macor glass composition	1,040–1,120°C, 4 h	4.8–5.5	Present work

material. Consequently, the hardness of the material decreases. In the present case, no crystallization is detected in the sample heat treated at 1,000°C for 4 h (see Fig. 2a). With increase in temperature to 1,040°C, large volume of fine mica crystals (low aspect ratio) has formed. These finer crystals get dissolved and re-precipitate on the larger crystals at higher temperature, so that the volume fraction of crystals is reduced. The aspect ratio and consequently, the interlocking between the crystals increases [14]. The hardness of the sample, heat treated at 1,040°C for 4 h is, for similar reason, better amongst the temperature variation batches i.e. because of the presence of finer crystals with lower interlocking (see Fig. 4).

A brief comparison with hardness properties of various other glass–ceramics has been made in Table 4 and such aspect is important to realize the potential of the presently investigated glass–ceramic samples. By varying the heat treatment temperature in the range of 1,000–1,120°C for 4 h, a range of hardness values, 2.7–3.6 GPa was measured in tetrasilisic fluoromica containing Dicor/MGC materials, with the highest recorded after heat treating at 1,000°C [27]. In a limited set of heat treatment experiments at 1,000–1,250°C on $8SiO_2$–$3Al_2O_3$–$3MgO$–$3MgF_2$–$(1-z)$ BaO–zK_2O–sLi_2O ('z' either 1 or 0 and 's' either 0.5 or 1.0) system, Henry and Hill measured similarly lower hardness in the range of 2.1–3.2 GPa [29]. These investigated materials exhibited a classical 'house-of-cards' microstructure, containing a varying volume fraction of Ba-fluorphlogopite and K-fluorophlogopite. It can be recalled here that one set of materials in the present study, heat treated at varying temperature, are also characterized by a similar 'house-of-cards' microstructure, containing interlocking mica crystals. In another study, Taruta et al. measured hardness values of 2.8 and 4.8 GPa in Mica–apatite glass–ceramics, containing 20% and 30% apatite [$Ca_{10}(PO_4)_6F_2$] crystalline phase respectively [30]. Such hardness values were reported to be superior to the commercial Macor material, having hardness of 3 GPa [31]. However, comparatively higher hardness in the range of 4–7 GPa were consistently measured by Goswami et al. in SiO_2–MgO–MgF_2 (MAS) glass–ceramics, which were heat treated at temperature upto 1,050°C. Irrespective of variation in starting glass composition, higher hardness of 6 GPa or more was obtained after heat treating at lower temperature of 600°C [32]. Similar higher hardness was also reported for MgO–Al_2O_3–SiO_2–TiO_2 glass–ceramics [21]. After heat treating the base glass at 1,080°C for 3 h, Wange et al. measured extremely high hardness of 9.5 GPa along with modest toughness of 4.3 MPa $m^{1/2}$ [21]. The major crystalline phases in those glass–ceramics include Mg–alumino silicate, Mg–alumino titanate etc. From the above discussion, it should be clear that the heat treatment of Macor glass composition in the temperature range of 1,040–1,120°C for 4 h, in the present study, enables us to obtain glass–ceramics with an appreciably modest hardness upto 5.5 GPa, which is higher than many of the earlier developed glass–ceramics materials.

4.2 Scratch induced damage resistance

From the experimental observations, as mentioned in Subsect. 3.3, it can be said that glass–ceramics containing 'spherulitic-dendritic' shaped crystals are relatively more resistant to scratch induced damage (see Figs. 8, 9). This can be attributed primarily to the characteristic crystal morphology. The dendrite structure actually results from the growth of the mica crystals in different directions, other than the primary axis of the initial mica plate. Therefore, they also have weaker interfaces and specific cleavage planes of fracture. Our understanding is that the presence of a large number of small mica crystals, in a very close space in the form of dendrites, allows the crack to deflect to a long path before breaking individual mica crystals (see Fig. 3a). This process is quite difficult and energy expensive as different mica plates will have their cleavage planes, differently oriented. This again causes the cracks to be deflected further as different crystals will have different cleavage planes oriented in different directions. Consequently, after breaking one mica plate, the crack has to move through the glass matrix in between mica plates.

Such phenomenon is evident from the electron microscopy image, as shown in Fig. 9. Also, the damage of the glass matrix in terms of spalling/pull out is not observed to any visible extent in time variation samples. Such phenomenon is, however commonly observed in case of temperature variation samples, consisting of plate like crystals (no dendrite at the end of the mica plates).

An interesting observation regarding the crystallography of fracture can be made by critically analyzing the preferred cleavage direction of these two types of mica crystals. The preferred cleavage direction of fluorophlogopite having plate shape morphology is through (001) plane as along this plane, large tetrahedrons are joined together by alkali ions. Also, the Fluorophlogopite mica plates are known to grow epitaxialy on prior norbegite crystals with their habit plane being (001)-type as this is the plane having lowest packing density. Thus, a postulate can be made based on these two facts that macroscopically, mica plates actually fracture perpendicular to their length. This indeed is found true by critically analyzing the crack propagation path or alternatively, the fracture direction in Fig. 7b. However, it is difficult to find exact crystallography of the cleavage plane in case of "spherulitic-dendritic" mainly due to the complex shape of these crystals. This is especially true for the "tree leave" structure at the end of individual mica plates. Nevertheless, each mica plates in the composite structure of "spherulitic-dendritic" crystals shows similar nature of fracture i.e. perpendicular to their length as do the plate shape crystals (see Fig. 9c). This observation further supports the proposed hypothesis regarding the damage behavior of the newly developed "spherulitic-dendritic" crystals.

From the above discussion, it can be said that if the amount of crystals be the same, the time variation samples with 'spherulitic-dendritic' crystals, composed of a number of mica plates with dendritic 'tree leaves' structure at the end of each mica plate, will be much more efficient in terms of crack blunting and crack deflection as compared to temperature variation samples with classical plate like crystals.

In order to strengthen this important point, some additional set of representative scratched/damaged microstructures for both temperature variation and time variation batch sample are presented in Fig. 10. After scratch testing under identical condition, large scratch induced material damage could be observed in case of the sample heat-treated at 1,120°C for 4 h (see Fig. 10a). The observation of 10–30 μm size fractured debrii can be made in Fig. 10a. Typical width of the scratch track is around 300 μm (see Fig. 10a). In contrast, electron microscopy image (see Fig. 10b) shows relatively less severe or deeper (refer Fig. 10a) scratch track on 'spherulitic-dendritic' crystal containing glass–ceramic (heat-treated at 1,000°C, 16 h).

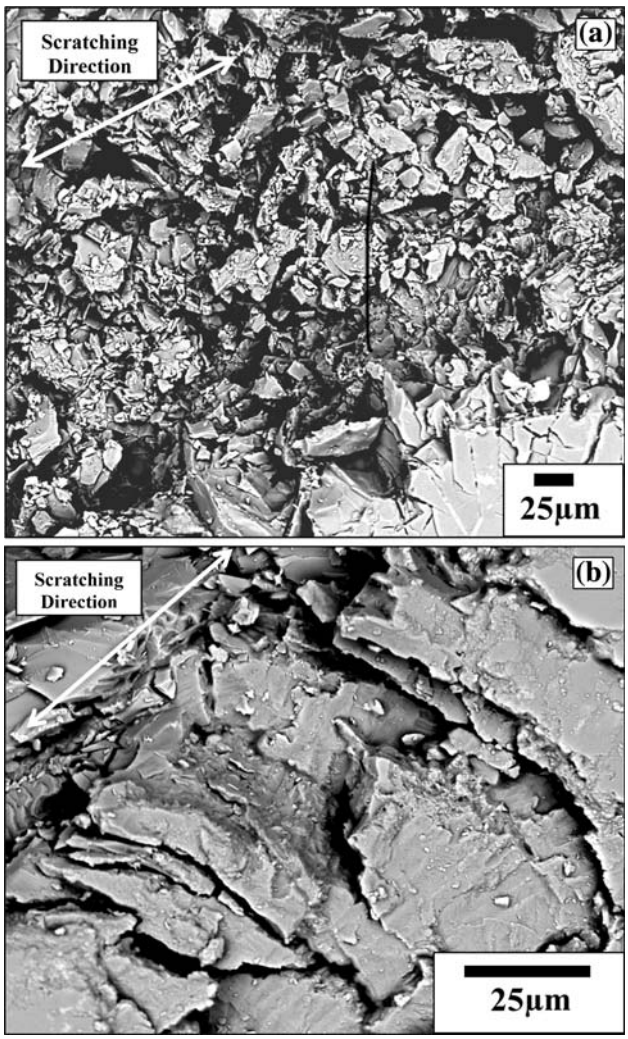

Fig. 10 **a** The accumulated debris particles on the surface of the scratched track (sample heat treated at 1,120°C for 4 h), illustrating severe damage behavior in artificial saliva environment, and **b** layering of damaged surface and evidence of scratching induced deformation and cracking in selected area of the scratched track (sample heat treated at 1,000°C for 16 h) when 50 N load was applied on the scratch indenter

The micrograph also reveals layered fracture, facilitated by large macrocracks. The above observation however supports the greater chance of ductile mode machinability in time variation samples, compared to the temperature variation one [16]. Such observations also reconfirm that the microstructure containing usual platelet shaped mica crystals are relatively poor resistant to scratch induced material damage.

The schematic representation of the crack-microstructure interaction is presented in Fig. 11, which provides a summary of phenomenon involved in 'spherulitic-dendritic' crystal-crack interaction. The important features include: (a) crack deflection and subsequent blunting by successive mica plates having individual cleavage planes at different

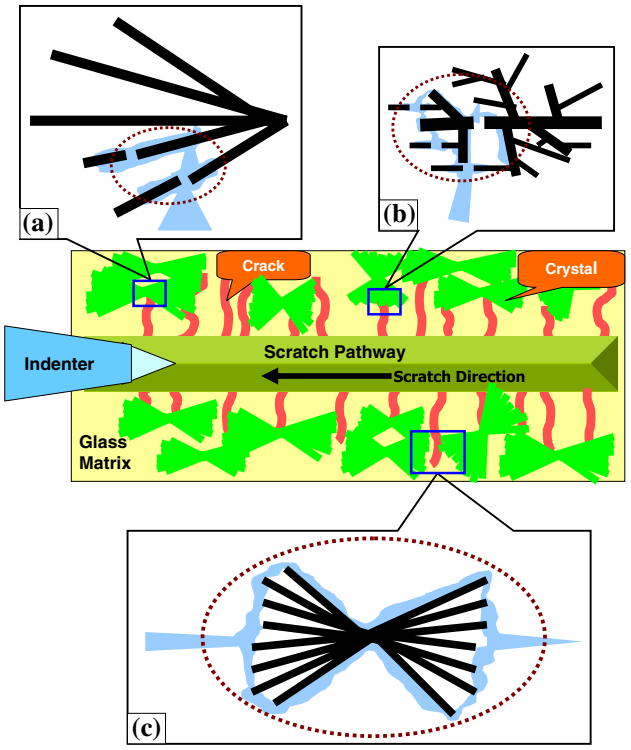

Fig. 11 Schematic of the crack-microstructure interaction in glass–ceramics, containing 'spherulitic-dendritic 'mica crystals; **a** showing the breaking of different mica plates (compressed together to form the original crystal) at different cleavage planes leading to effective crack blunting (*shown by the dotted circle*); **b** showing the crack blunting by the same mechanism as that shown in **a** of dendritic structure at the end of each of the mica plates (*shown by the dotted circle*), and **c** both the mechanisms **a** and **b** leads to extensive crack deflection (*shown by the dotted circle*)

orientations, (b) crack deflection and subsequent blunting by dendritic structure at the end of each mica plates and (c) large amount of crack deflection by spherulitic-dendritic crystals, having larger crystal–glass interface than plate like crystals.

5 Conclusions

Based on the experimental investigation of hardness property as well as the scratch–microstructure interaction of the glass ceramics with randomly oriented, interlocked plate like mica plates as well as unique 'spherulitic-dendritic' shaped morphology reveals some interesting results and the interpretation of such results lead to some of the following major conclusions:

(a) The glass–ceramic material containing highest amount of crystal (heat treated at 1,040°C for 4 h) exhibits highest hardness of 5.5 GPa. The hardness measurements of a limited number of glass ceramic samples do not reveal any statistically relevant inverse relationship with the crystal volume fraction. The presence of radial-median cracks at the edge of the indentation reveals the classical brittle nature of the glass–ceramic material.

(b) The microstructural observations of the scratched glass–ceramic samples reveal that the glass ceramic containing 'plate' likes anisotropic crystals can experience extreme brittle fracture behavior, leading to large amount of debris formation (sizes of upto 100 μm). In contrast, the layering of damages layers occurs in case of glass ceramic with 'spherulitic-dendritic' shaped crystals.

(c) Importantly, the experimental results indicate that the 'spherulitic-dendritic' shaped crystals can stop the crack propagation more effectively than the plate like crystals, because of the larger weak interface with the glass matrix helping in more crack deflection; when both are scratched in artificial saliva solution at 50 N load. The dendritic 'tree leaves' structure at the end of the 'spherulitic-dendritic' crystals is found to help in crack blunting. Both of these mechanisms would lead to the greater machinability in the time variation samples, compared to the temperature variation samples.

References

1. Vogel W, Höland W, Kaumann K. Development of machinable bioactive glass–ceramics for medical uses. J Non-Cryst Solids. 1986;80:34–51.
2. Chaudhry MA, Jonscher AK. High-temperature dielectric properties of ruby mica perpendicular to the cleavage planes. J Mater Sci. 1988;23:208–16.
3. Holand W, Vogel W. Machineable and phosphate glass ceramics. In: Hench LL, Wilson J, editors. Introduction to bioceramics. Singapore: World Scientific; 1993. pp. 125–38.
4. Holand W, Beall G. Glass–ceramic technology. Westerville, OH: The American Ceramic Society; 2002.
5. Cheng K, Wan J, Liang K. Crystallization of R_2O–MgO–Al_2O_3–B_2O_3–SiO_2–F (R = K^+, Na^+) glasses with different fluorine sources. Mater Lett. 2001;47:1–6.
6. Hoche T, Habelitz S, Avramov I. Crystal morphology engineering in SiO_2–Al_2O_3–MgO–K_2O–Na_2O–F^- mica glass–ceramics. Acta Mater. 1998;PII:S1359–6454; 00424–8.
7. Gebhardt A, Hoche T, Carl G, Khodos II. TEM study on the origin of cabbage-shaped mica crystal aggregates in machinable glass–ceramics. Acta Mater. 1999;47(17):4427–34.
8. Quinn JB, Sundar V, Lloyd IK. Influence of microstructure and chemistry on the fracture toughness of dental ceramics. Dent Mater. 2003;19:603–11.
9. Höche T, Habelitz S, Khoodos II. Origin of unusual fluorophlogopite morphology in mica glass–ceramics of the system SiO_2–Al_2O_3–MgO–K_2O–Na_2O–F_2. J Cryst Growth. 1998;192:185–95.
10. Boccaccini AR. Machinability and brittleness of glass–ceramics. J Mater Process Technol. 1997;65:302–4.

11. Ma XP, Li GX, Shen L, Jin ZH. Ductile-mode material removal of a mica–glass–ceramic. J Am Ceram Soc. 2003;86(6):1040–2.
12. Lawn BR, Padture NP, Cai H, Guiberteau F. Making ceramics 'ductile'. Science. 1994;263:1114–6.
13. Baik DS, No KS, Chun JS, Cho HY. Effect of the aspect ratio of mica crystals and crystallinity on the microhardness and machinability of mica glass–ceramics. J Mater Process Technol. 1997;67:50–4.
14. Grossman DG. Machinable glass–ceramics based on tetrasilicic mica. J Am Ceram Soc. 1972;55(9):446–9.
15. Xu HK, Jahanmir S. Scratching and grinding of a machinable glass–ceramic with weak interfaces and rising T-curve. J Am Ceram Soc. 1995;78:497–500.
16. Flanders LA, Quinn JB, Wilson OC Jr, Lloyd IK. Scratch hardness and chipping of dental ceramics under different environments. Dent Mater. 2003;19:716–24.
17. Roy S, Basu B. On the development of two characteristically different crystal morphology in SiO_2–MgO–Al_2O_3–K_2O–B_2O_3–F glass–ceramic system. J Mater Sci: Mater Med. 2008;20(1): 51–66.
18. Roy S, Basu B. In vitro dissolution behavior of SiO_2–MgO–Al_2O_3–K_2O–B_2O_3–F glass–ceramic system. J Mater Sci: Mater Med. 2008;19:3123–33.
19. Roy S. Microstructure development and in-vitro properties of Macor Glass–ceramic, M. Tech Thesis, IIT Kanpur, India, May 2005.
20. Guedes A, Pinto AMP, Vieira M, Viana F. Multilayered interface in Ti:Macor® machinable glass–ceramic joints. Mater Sci Eng A. 2001;301:118–24.
21. Wange P, Höche T, Rüssel C, Schnapp JD. Microstructure-property relationship in high-strength MgO–Al_2O_3–SiO_2–TiO_2 glass–ceramics. J Non-Cryst Solids. 2002;298:137–45.
22. Karamanov A, Pelino M. Evaluation of the degree of crystallization in glass–ceramics by density measurements. J Eur Ceram Soc. 1999;19:649-54.
23. Roy S, Basu B. Mechanical and tribological characterization of human tooth. Mater Charact. 2008;59:747–56.
24. Li H, Zhou ZR. Wear behaviour of human teeth in dry and artificial saliva conditions. Wear. 2002;249:980–4.
25. Uhlmann DR. Crystal growth in glass-forming systems—a review. In: Hench LL, Freiman FW, editors. Advances in nucleation and crystallization in glasses, special publication 5. Columbus, OH: American Ceramic Society; 1971. pp. 91–115.
26. Cripps ACF, Lawn BR. Indentation stress–strain curves for 'quasi-ductile' ceramics. Acta Mater. 1996;44(2):519–27.
27. Peterson IM, Wuttiphan S, Lawn BR, Chyung K. Role of microstructure on contact damage and strength degradation of micaceous glass–ceramic. Dent Mater. 1998;14(1):80–9.
28. Saraswati V, Raoot S. Machinable mica-based glass–ceramic. J Mater Sci. 1992;27:429–32.
29. Henry J, Hill RG. The influence of lithia content on the properties of fluorphlogopite glass–ceramics. II. Microstructure hardness and machinability. J Non-Cryst Solids. 2003;319:13–30.
30. Taruta S, Mukoyama K, Suzuki SS, Kitajima K, Takusagawa N. Crystallization process and some properties of calcium mica–apatite glass–ceramics. J Non-Cryst Solids. 2001;296:201–11.
31. Davis JB, Marshall DB, Housley RM, Morgan PED. Machinable ceramics containing rare-earth phosphates. J Am Ceram Soc. 1998;81:2169–75.
32. Goswami M, Sarkar A, Mirza T, Shrikhande VK, Sangeeta, Gurumurthy KR, et al. Study of some thermal and mechanical properties of magnesium aluminium silicate glass–ceramic. Ceram Int. 2002;28:585–92.